Construction and Building Materials 280 (2021) 122508

Contents lists available at ScienceDirect

Construction and Building Materials

journal homepage: www.elsevier.com/locate/conbuildmat

Integrated experimental and numerical study on flexural properties of cross laminated timber made of low-value sugar maple lumber

Yunxiang Ma [a], Munkaila Musah [b], Ruizhe Si [a], Qingli Dai [a,*], Xinfeng Xie [b], Xiping Wang [b,c], Robert J. Ross [b,c]

[a] Department of Civil and Environmental Engineering, Michigan Technological University, United States
[b] College of Forest Resources and Environmental Science, Michigan Technological University, United States
[c] USDA Forest Service, Forest Products Laboratory, United States

HIGHLIGHTS

- Flexural properties of CLT panels made with low-value sugar maple has been studied.
- Melamine provided better bonding than Resorcinol but not much on flexural properties.
- Stronger outer layers strengthen the overall major direction flexural performance of CLT.
- Studied layups provided better bending and shear performance than standard layup E1.
- The finite element model provided satisfactory estimation based on lamination data.

ARTICLE INFO

Article history:
Received 1 June 2020
Received in revised form 21 January 2021
Accepted 24 January 2021

Keywords:
Cross-laminated timber (CLT)
Low-value hardwood
Flexural properties
Static bending test
Finite element modeling

ABSTRACT

The objective of this study is to examine the mechanical performance of cross laminated timber (CLT) panels made of low-value sugar maple under out of plane loads through mechanical tests and numerical simulation. The laminations were sorted into High and Low classes based on the measured modulus of elasticity (MOE). Two 3-layer sugar maple CLT layups as High-Low-High and Low-High-Low glued with resorcinol-based adhesive and one CLT layup of High-Low-High glued with melamine-based adhesive were prepared. Block shear, long-span bending (span-to-depth ratio of 33:1) and short-span bending (5.5:1) tests were conducted to evaluate the bonding, flexural and shear behavior of these low-value sugar maple CLTs. With a limited sample size, the lab-manufactured low-value sugar maple CLT provided a 50% to 80% higher MOE and at least two times higher MOR than CLT type E1 from APA/PRG 320. Similar MOE and MOR improvements were found by comparing CLT made with other species from literatures. The finite element simulation of bending tests was conducted with the orthogonal constitutive law and the progressive damage model based on the calibrated material properties parameters from lumber rating and references. The simulation results on each CLT panel type have a reasonable comparison with experimental test data. Therefore, these integrated experiment and simulation methods can provide detailed mechanical behaviors of the low-value sugar maple CLT, which can also be applied to other CLT species and layup.

1. Introduction

Cross-laminated timber (CLT) is a novel engineered timber product that expands the structural utilization of mass timber into two-dimensional components with its orthogonal flatwise behavior [1]. Mass timber structure with CLT components has become a competitive option for the construction of mid- to high-rise buildings up to 30 stories [2]. As CLT market thrives in the US, CLT product standard (ANSI/APA PRG 320) [3] has been developed to guide the fabrication and construction of CLT panels. The typical cross-section of CLT panels has at least three layers of boards that are orthogonal to their adjacent layers [1]. Traditionally, CLT panels are produced from softwood lumber. With an increased interest in using CLT products in both commercial and residential constructions, the effort is underway in the forest products industry to fully develop a CLT manufacturing industry country-wide. This will require the use of a variety of regional species. At this time, the product standard for CLT in the United States, ANSI/APA PRG 320

* Corresponding author.
E-mail addresses: yma2@mtu.edu (Y. Ma), mmusah@mtu.edu (M. Musah), ruizhes@mtu.edu (R. Si), qingdai@mtu.edu (Q. Dai), xinfengx@mtu.edu (X. Xie), xiping.wang@usda.gov (X. Wang), robert.j.ross@usda.gov (R.J. Ross).

https://doi.org/10.1016/j.conbuildmat.2021.122508
0950-0618/

[3], does not apply to CLT manufactured from hardwood lumber. Given this situation, further research is necessary to justify the inclusion of hardwood species into the standard.

In the study of CLT manufacturing, including more wood species is considered as a main approach to expand the source of timber [4]. Some studies have been conducted around the world to examine the potential use of hardwood species in CLT products. For example, Ehrhart et al. investigated a number of European hardwood species, including poplar (*Populus* spp.), silver birch (*Betula pendula* Roth), European beech (*Fagus sylvatica* L.), and European ash (*Fraxinus excelsior* L.) through planar shear tests and proved that these species have a potential to be used in CLT manufacturing [5,6]. Currently, low-value hardwood is primarily used as pallet parts, railroad ties, etc. [7]. A growing interest has been rising in the Great Lake region to use low-value sugar maple (*Acer saccharum* Marsh) in CLT. Popular hardwood species such as yellow poplar [8,9], birch [10], beech [11] have been examined for their utilization in CLT. In the Great Lakes area, forest stocks of sugar maple with superior properties are growing [12], which could be a potential source for CLT manufacture.

The flexural strength (MOR) and stiffness (MOE) of CLT are critical properties that influence the design and applications of CLT panels for mass timber structures. The current standard for performance-rated CLT panels recommends that the flexural properties of CLT be evaluated through long-span flexural tests with a span-to-depth ratio of around 30 [3,13]. He et al. [14] conducted flexural tests with a span of 27.85 times depth for the CLT flexural performance. Hindman and Bouldin [15] tested CLT samples with a span-to-depth ratio of 27:1 in bending. Short-span bending test with the span-to-depth ratio of 4 to 6 is recommended to determine the shear properties of CLT panels according to ASTM D198 [13] and PRG 320 [3]. Flores et al. [16] studied the shear properties of CLT panels through actual experiments and simulated short-span flexural tests. The planar shear test is another approach to evaluate the shear resistance of the CLT [17,18], which is considered as the most appropriate one in Europe [19]. However, the result in one study indicated that the planar shear test and the short-span bending test provide comparable data [20]. In this study, the short-span bending test was applied to examine the shear and bending properties of sugar maple CLT. To evaluate a new CLT product, experimental program including both the long-span and short-span test were used for the examination of mechanical properties [21]. The combined test program was also applied in this study.

Finite element (FE) simulation is a viable and efficient tool to comprehensively analyze and estimate the CLT mechanical properties. He et al. [14] investigated the bending and compressive properties of CLT made from Canadian hemlock with both experimental testing and finite element analysis. The comparison between the experimental and numerical results illustrated that the models could predict the stiffness and strength of CLT panels in bending. Chen and Lam [22] investigated the flexural performance of CLT panels with different interlayer angles made from Spruce-Pine-Fir (SPF) and a box-based CLT floor system by integrated experimental and numerical analysis. The model in the study is capable of providing a prediction of the combined structure system under out-of-plane loading. In order to capture the timber damage behavior in the finite element models, the Hashin damage criteria [23] have been widely used. Gharib et al. [24] established a feasible constitutive law to the modeling of arbitrarily orientated timber with the Hashin damage model as the failure criteria and validated with experimental data. Brank et al. [25] demonstrated a procedure of designing ribbed CLT plates, in which the design is optimized by the failure analysis with the Hashin failure criteria. It is approved that Hashin damage criteria can capture the orthogonal distribution of the timber stress strength. Hashin damage criteria are chosen to simulate the failure of CLT samples in this study.

The scope of this study is to investigate the flexural performance of the lab manufactured CLT made from low-value sugar maple (Acer saccharum) boards with experiment and simulation analysis. Therefore, the primary objective of this study is to evaluate the flatwise bending and shear properties of the CLT panels through the integrated experimental tests and numerical simulation. As presented in Section 2, the sugar maple lumber were firstly grouped based on the E-rating. The CLT samples were then manufactured accordingly in two layups with two common adhesives. In Section 3, the block shear test, long-span and short span bending tests were conducted for the evaluation of the mechanical properties. The results and comparison with the reference values are presented in Section 4. As shown in Section 5, the orthogonal material model and the progressive damage model were applied and the input parameters were calibrated based on the rating of the lumber to provide a close estimation of the mechanical properties of certain sample group. Section 6 presents the simulation of the long and short span tests and the correlated comparison with test results. The flexural performance of CLT panels made from low-value sugar maple in major direction were evaluated with the experimental and numerical investigation.

2. Lab preparation of CLT panels with sugar maple boards

All the boards were kiln dried sugar maple harvested in Great Lake Region. They were visually graded as No.1 common according to the National Hardwood Lumber Association (NHLA) grading rules. The boards have been surfaced to a uniform thickness of 23 mm. The width of the boards varied from 71 mm to 213 mm. All the boards used for manufacturing the CLT panels were conditioned to 12 ± 3% moisture content (MC).

2.1. E-rating of boards

The sugar maple boards were nondestructively tested to obtain dynamic MOE using a transverse vibration test method, according to ASTM D6874 [26]. Each board was placed onto a support system, with edge support at one end and a point support through loading cell at the other end, as shown in Fig. 1. Following a vertical impact at the mid-span, the board was set into free vibration. The equipment measured the weight and change of support reactions by the loading cell and recorded the vibration frequency. With the input dimensions of each lumber, the bending modulus of each board (MOE_{TV}) can be calculated in Eq. (1).

$$MOE_{TV} = \frac{WL^3f^3}{Kbh^3} \quad (1)$$

W and f are the weight and vibration frequency measured with the load cell, L is the span length, K is a calibration constant, b and h are the width and depth of the lumber cross-section, separately. The tested vibration MOE_{TV} of each lamination and the dimensions were recorded to track the specific layup of each panel. The low-value sugar maple have an average MOE of 14,230 MPa and the Coefficient of Variance of 31.7% [27]. Based on the test results, the laminations were divided into two groups with similar size: High (H, $MOE_{TV} > 1.38 \times 10^4$ MPa (2×10^6 psi)) and Low (L, $MOE_{TV} < 1.38 \times 10^4$ MPa (2×10^6 psi)).

2.2. CLT panel fabrication and sample types

The tested laminations were first trimmed and glued into CLT panels of 2438 mm (8 ft) long and 609 mm (2 ft) wide according to the designed layups. A total of 8 CLT panels were manufactured,

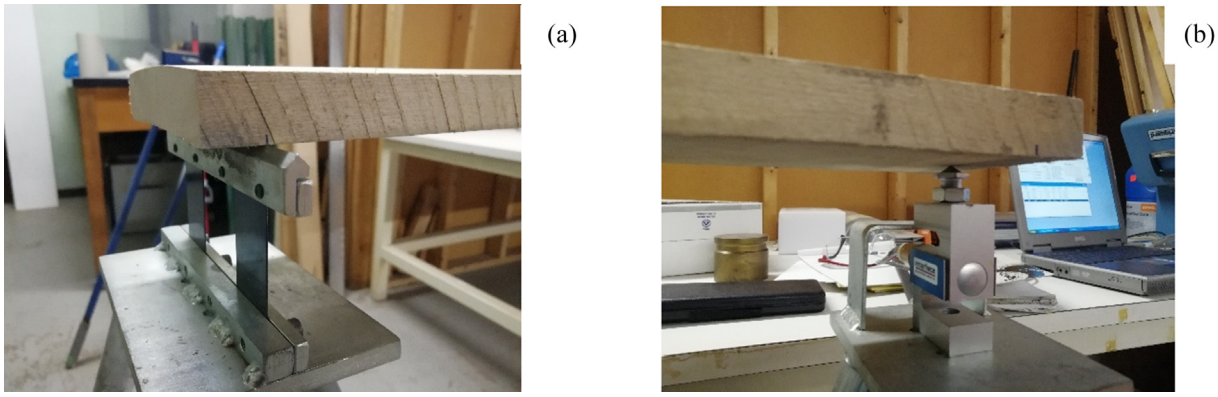

Fig. 1. Test setup for conducting transverse vibration test. (a) flexible edge support (b) point support through a load cell.

including three panels with the High-Low-High (HLH) layup glued by melamine–formaldehyde (M), three panels with the High-Low-High (HLH) layup glued by resorcinol–formaldehyde adhesive (R), and two CLT panels with the Low-High-Low (LHL) layup glued by resorcinol formaldehyde adhesive.

The groups and the average MOE_{TV} of the laminations of each layer are listed as MOE_{TV} in Table 1. The CLT panels were then cut into samples for long-span third point flexural test (sample type L) and short-span three-point flexural test (sample type S). For the long-span flexural test, the samples were 305 mm (1 ft) wide and 2438 mm (8 ft) long with the original thickness of 69 mm. The sample type S for short-span flexural test were 457 mm (18 in.) long, 254 mm width, with a constant thickness. Three type L samples and six type S samples were cut from each CLT panel type. For instance, the first MHLH (M is the adhesive type; HLH is layup type) panel was cut into one long-span sample (type L) coded as MHLH-L1 and two short-span sample (type S) coded as MHLH-S1 and MHLH-S2.

3. Mechanical property tests of the CLT panels

3.1. Block shear test

The block shear test was conducted to evaluate the bonding strength in the CLT panels. The test were conducted based on ASTM D905 [28] with 8 samples from each of the 3 CLT groups. Specimens were prepared according to the ANSI PRG 320 [3] standard based on the ASTM D905 [28]. The samples have a length of 50 mm, a total width of 63.5 mm and containing all the three layers in the shape of 12.7 mm wide stairs. The testing was done at a loading rate of 2 mm/min in a universal testing machine with 1000 kN (225 kips) strength. The percentage of wood failure was estimated immediately after test according to ASTM D5266 [29] to examine the bonding quality. The load was measured with the loading cell at the loading head. The shear strength was calculated by dividing the maximum load with the bonding area. The shear strength was recorded for the CLT groups accordingly. The average shear strength and the average wood failure percentage were calculated to present the overall bonding properties of each layup.

3.2. Long-span bending test and data processing

The bending properties of the CLT beam specimens were evaluated through four-point static bending tests in accordance with ASTM D198 [13]. The CLT beam samples with a length of 2438 mm, a width of 305 mm, and the depth of 69 mm were used for the long-span flexural test. A total of eight CLT beams were tested, including 3 MHLH beams, 3 RHLH beams, and 2 RLHL beams, as shown in Table 1. The tested CLT beam samples were used to evaluate the effects of different CLT layups based on MOE grouping and type of adhesives on the bending performance of CLT beams. The procedures of the long-span flexural test were determined according to the ASTM D198 standard [13]. During the flexural test, the loading rate was fixed at 10.16 mm/min (0.4 in/min) for all the tested samples. The setup of the loading frame and detailed dimension of the long-span sample are shown in Fig. 2 (a) and (b), respectively. The span of the tested CLT beam was 2286 mm, and the overhangs (the length from the center of the supports to the nearest end of the samples) were 76 mm. The span-to-depth ratio is 33.3:1, which fulfilled the requirement in the ASTM D198 standard [13]. The mid-span displacement was measured with a pair of LVDTs. The average reading was recorded as the mid-span displacement to eliminate the effect of torsion. The vertical load applied by the actuator was recorded as the total load on the sample.

The shear deformation can be neglected considering the large span-to-depth ratio[30]. Then, the modulus of elasticity (MOE_{CLT}) of the panel can be calculated as:

$$MOE_{CLT} = \frac{Pa}{2\Delta_{max} I}\left(\frac{l^2}{8} - \frac{a^2}{6}\right) \quad (2)$$

Table 1
Average MOE_{TV} of laminations in each layer of each CLT sample (unit: MPa).

Sample type and numbers	Longitudinal layers		Transverse layer	Average: longitudinal layers	Average: transverse layer
	Top	Bottom	Middle		
MHLH-(L1, S1-2)	1.85×10^4	1.75×10^4	7.39×10^3	1.75×10^4	7.24×10^3
MHLH-(L2, S3-4)	1.98×10^4	1.67×10^4	6.84×10^3		
MHLH-(L3, S5-6)	1.54×10^4	1.69×10^4	7.50×10^3		
RHLH-(L1, S1-3)	1.49×10^4	1.71×10^4	1.20×10^4	1.69×10^4	1.12×10^4
RHLH-(L2, S4)	1.69×10^4	1.59×10^4	1.10×10^4		
RHLH-(L3, S5-6)	1.71×10^4	1.77×10^4	1.15×10^4		
RLHL-(L, S1-4)	9.65×10^3	8.49×10^3	2.04×10^4	8.07×10^3	1.95×10^4
RLHL-(L, S5-6)	6.84×10^3	7.29×10^3	1.86×10^4		

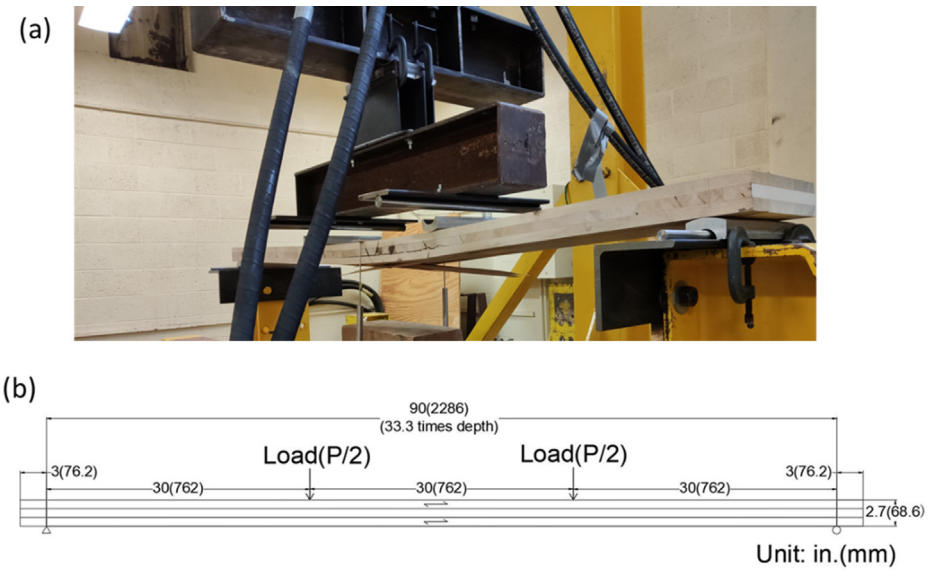

Fig. 2. Long-span flexural test setup. (a) loading frame and fixtures; (b) dimension of the long span samples.

where P is the peak load of the test, a is the distance between the center of the support to the nearest loading location, Δ_{max} is the maximum displacement of the beam during the test, l is the beam span, and I represents the moment of inertia of the CLT beam.

When the sample reaches the peak load, the modulus of rupture ($MOR_{CLT\text{-}L}$) tested in long-span test is defined as:

$$MOR_{CLT-L} = \frac{My}{I} \tag{3}$$

where M is the mid-span moment of the beam ($M = P \times a/2$) and y is the distance from beam bottom to the neutral axis and half depth was used in this study.

3.3. Short-span bending test and data processing

The short-span bending tests were conducted to evaluate the shear properties of three types of CLT beams, MHLH, RHLH, and RLHL. The static bending tests were conducted using the center-point loading in accordance with ASTM D198 [17], with a test span of 381 mm. The short-span bending tests were conducted on the samples based on the recommendation of the ASTM D198 standard [13]. Six samples were prepared for each type of CLT panels. The loading rate of 10.16 mm/min (0.4 in/min) was used for the bending tests to make sure the testing time was around 10 min, which is recommended by the ASTM D198 standard [13]. The setup of the loading frame and detailed sample dimensions of the short-span test are shown in Fig. 3 (a) and (b), respectively. The span of the tested CLT beams was 381 mm with 38 mm of overhang. The three-point loading, in which a single load was applied at the mid-span of the samples, was used for the short-span bending test. The aluminum loading head has a contact surface of 305 mm long, and 63.5 mm wide. The contact surface is designed to be curvature with radius of 190.5 mm (2.78 times of sample thickness) to eliminate the possible local compressive failure. Two steel tubes with a diameter of 50.8 mm were used as the supports of the short-span beams. The supports were rested at a distance of 381 mm and supported by a 305 mm wide channel beam.

The shear analogy method is the recommended method for calculating CLT design values in the US CLT handbook [30]. The test data was analyzed according to the shear analogy methods. Accordingly, the shear stiffness can be calculated as:

$$GA_{eff-test-S} = \frac{K_s EI_{eff}}{\left(\frac{EI_{eff}}{EI_{app-test-S}} - 1\right)l^2} \tag{4}$$

where $EI_{app\text{-}test\text{-}S}$ is the apparent bending stiffness, which is calculated as the flexural stiffness of the short span sample considering no shear effective; K_s is the shear influence factor, which is 14.4 for pinned-ends three-point bending beams; EI_{eff} is the effective bending stiffness of the combination of all layers, which can be calculated as:

$$EI_{eff} = \sum_{i=1}^{n} E_i b_i h_i^3/12 + \sum_{i=1}^{n} E_i A_i z_i^2 \tag{5}$$

in which E_i is elastic modulus of the i^{th} layer in the panel longitudinal direction, h_i and z_i are the depth of each layer and the distance in between the layer neutral axis and the panel neutral axis. The width (b_i) is set as unit length, and the area (A_i) is calculated accordingly.

The overall shear modulus of the panel is necessary to be calculated in order to compare in between the panels with different depth, the shear modulus (G) can be expressed as:

$$G = GA_{eff-test-S}/A \tag{6}$$

4. Mechanical test results

4.1. Bonding property from block shear tests

The bonding strength and wood failure percentage obtained from the block shear test are as shown in Fig. 4. Since the wood failure percentage was over 85% for the all three types of sample, the bonding quality can be considered adequate. According to the block shear test results, the shear strength of the bonded surface for Melamine is 4.7 MPa, while it is separately 2.97 MPa and 2.89 MPa for the RHLH and RLHL samples. It seems that the direct shear strength of Melamine bonded interface is much higher than that with Resorcinol.

4.2. Flexural properties of long-span bending tests

The results of the long-span bending tests on CLT beams are shown in Table 2. The average modulus of elasticity of the CLT

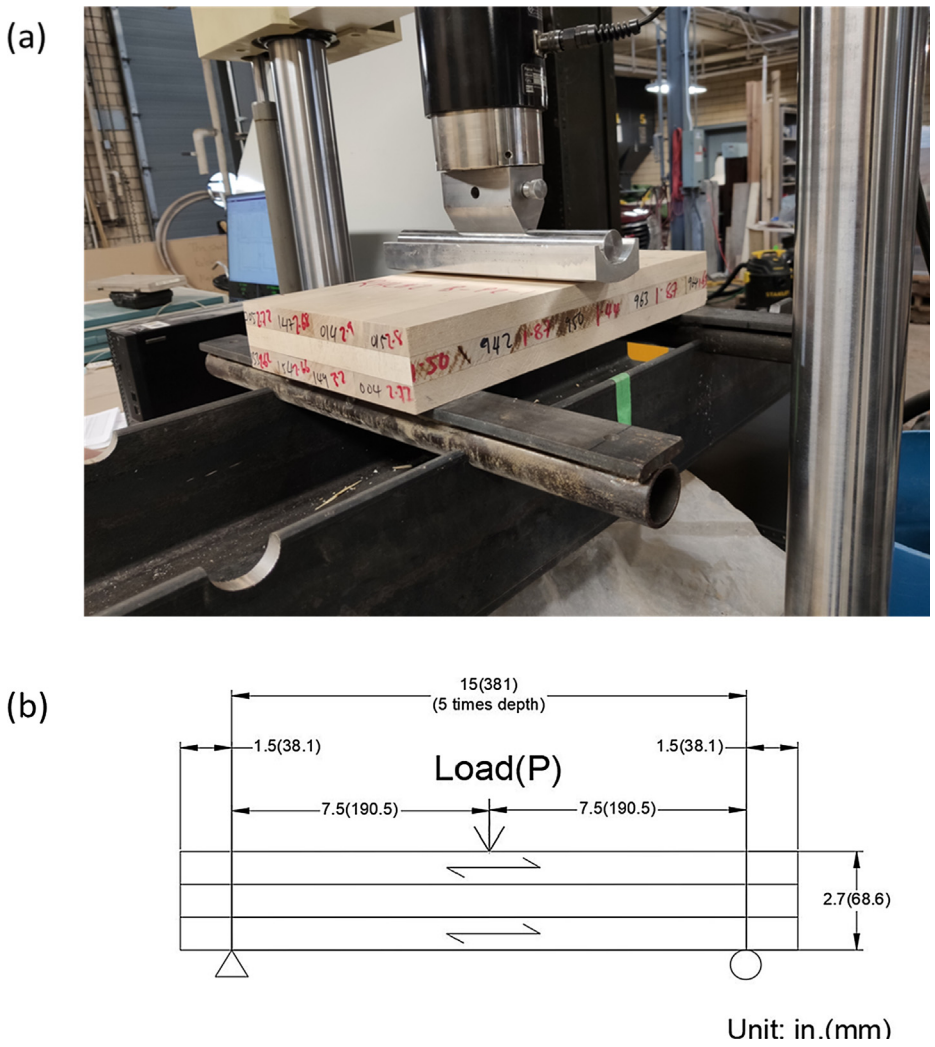

Fig. 3. Short span bending test setup. (a) loading frame and fixtures; (b) dimension of the short span samples.

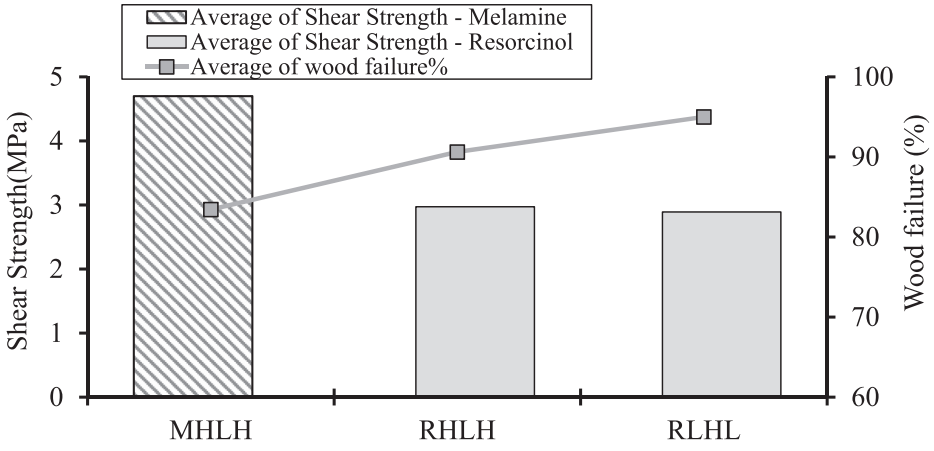

Fig. 4. Results of block shear tests.

beams was 18.10 GPa for MHLH-L, 17.90 GPa for RHLH-L, and 18.60 GPa for RLHL-L respectively. The Coefficient of Variation of the MOE is relatively small comparing with the MOR, which is 2.07% and 2.77% for the HLH layup, and 9.14% for the RLHL-L. No significant difference was found in measured MOE among these three types of CLT panels. The result indicates that differences in layup and adhesives had minor effect on the average modulus of elasticity of the panels.

Though the variance of RHLH (16.98%) is much larger than MHLH (3.24%), the average of bending strength of the RHLH-L CLT beams was improved by 12.6% when comparing with the MHLH-L CLT beams, indicating that the resorcinol adhesive may

Table 2
Long-span bending test results.

Sample ID	MOE_{CLT} (GPa)	Average MOE_{CLT} (GPa)	Average MOE_{CLT} CoV	MOR_{CLT-L} (MPa)	Average MOR_{CLT-L} (MPa)	MOR_{CLT-L} CoV	Failure mode
MHLH-L1	18.50	18.10	2.07%	74.30	77.20	3.24%	Bottom splinter
MHLH-L2	17.60			80.40			Bottom splinter
MHLH-L3	18.20			76.80			Shear in middle layer
RHLH-L1	18.30	17.90	2.77%	66.90	86.90	16.98%	Shear in middle layer
RHLH-L2	18.20			91.90			Shear in middle layer
RHLH-L3	17.20			102.00			Shear in middle layer
RLHL-L1	16.90	18.60	9.14%	72.80	79.20	8.02%	Bottom splinter
RLHL-L2	20.30			85.50			Shear in middle layer

provide better bending strength in CLT panels than melamine adhesive. The average bending strength of the RLHL-L CLT beams was 8.9% smaller than the results of the RHLH-L group. The layups changes in these two types of CLT beams had a major impact on the bending strength. The damage of the samples was initiated with either shear failure in the center layer or tension failure in the bottom layer. There is no correlation found in between the layup or adhesive and the damage mode.

4.3. Flexural and shear properties of short-span bending tests

The shear modulus (G) and shear strength (MOR_{CLT-S}) of the three types of CLT beams are shown in Table 3. The Coefficient of Variation (CoV) of the tested shear modulus is 6.93% to 17.13%, while the CoV of shear strength is 13.48–27.63%. The CLT beams glued with melamine-based adhesive (MHLH-S) presented an average shear modulus 4.6% smaller than the CLT beams with resorcinol-based adhesive (RHLH-S). Meanwhile, the average shear strength of the MHLH-S samples was improved by 3.4% comparing with the RHLH-S. For different layups, the average shear modulus of the RHLH-S was 9.06% higher than the RLHL-S. The average MOR_{CLT-S} of the RLHL-S was only 1.7% lower than that of the RHLH-S.

4.4. Effects of adhesives on panel bending modulus (MOE_{CLT}), shear modulus (G), and modulus of rupture (MOR_{CLT-L} and MOR_{CLT-S})

The results of the shear modulus (G), bending modulus of elasticity (MOE_{CLT}), and modulus of rupture (MOR_{CLT-L}) of the CLT panels with different types of adhesives are shown in Fig. 5 (a), (b), and (c), respectively. Fig. 5 (a) and (b) illustrate that there is no obvious difference in the MOE_{CLT} and shear modulus of between the CLT panels with different types of adhesive. For long-span tests, the tested MOR_{CLT-L} of the CLT panels with melamine adhesive was improved by 12.6% comparing with CLT panels glued with resorcinol adhesive. However, for the short span samples, the difference of the MOR_{CLT-S} between melamine glued samples and resorcinol glued samples is minor, as shown in Fig. 5 (c). Comparing with the block shear test results, in which the Melamine bonded interfaces provided higher direct shear strength than Resorcinol interfaces, the results illustrated that the interface bonding strength does not have considerable influence to the panel flexural strength of the samples. Meanwhile, the damage was observed mostly initiated inside the layer according to the recorded damage modes. Therefore, the adhesive bonding of the lab-made low-value sugar maple CLT samples provided adequate strength to avoid debonding. The observed differences should be the result of variance in lumber properties.

4.5. Effects of CLT layups on panel bending modulus (MOE_{CLT}), shear modulus (G), and modulus of rupture (MOR_{CLT-L})

The results of the MOE_{CLT}, shear modulus and MOR_{CLT-L} of the CLT panels with different layups are summarized in Fig. 6 (a), (b), and (c), respectively. Fig. 6 presents that the MOR_{CLT-L} is affected by the panel layup, while the MOE_{CLT} and shear modulus are not affected much by the layup. As shown in Fig. 6 (b), the RHLH type had 6.7% higher average shear modulus than the RLHL type CLT beam. It might because the RHLH CLT panels contained more "High" layers than the RLHL type panels. On the other hand, the average MOE of the RLHL group was 4% higher than that of the RHLH group. Considering the variance of the sample results as shown in Table 2 and Table 3, the observed influence of layup to the modulus is limited. For both long-span and short-span CLT beam, the MOR_{CLT-L} of the RHLH was higher than that of the RLHL. The improvement of the MOR_{CLT-L} was more in long-span beams,

Table 3
Shear properties of the CLT beams obtained from short-span bending test.

Sample type	G (MPa)	Average G (MPa)	G CoV	MOR (MPa)	Average MOR (MPa)	MOR CoV
MHLH-S1	104.02	93.20	17.13%	49.09	48.51	13.48%
MHLH-S2	114.12			38.03		
MHLH-S3	90.51			60.05		
MHLH-S4	94.17			49.85		
MHLH-S5	62.13			45.15		
MHLH-S6	94.24			48.88		
RHLH-S1	106.42	97.73	6.93%	44.96	46.92	16.43%
RHLH-S2	96.43			42.41		
RHLH-S3	84.82			41.43		
RHLH-S4	99.30			63.11		
RHLH-S5	102.93			40.85		
RHLH-S6	96.47			48.75		
RLHL-S1	93.44	88.69	12.50%	56.64	46.11	27.63%
RLHL-S2	75.58			39.96		
RLHL-S3	71.70			27.27		
RLHL-S4	97.65			64.70		
RLHL-S5	101.37			51.68		
RLHL-S6	92.42			36.42		

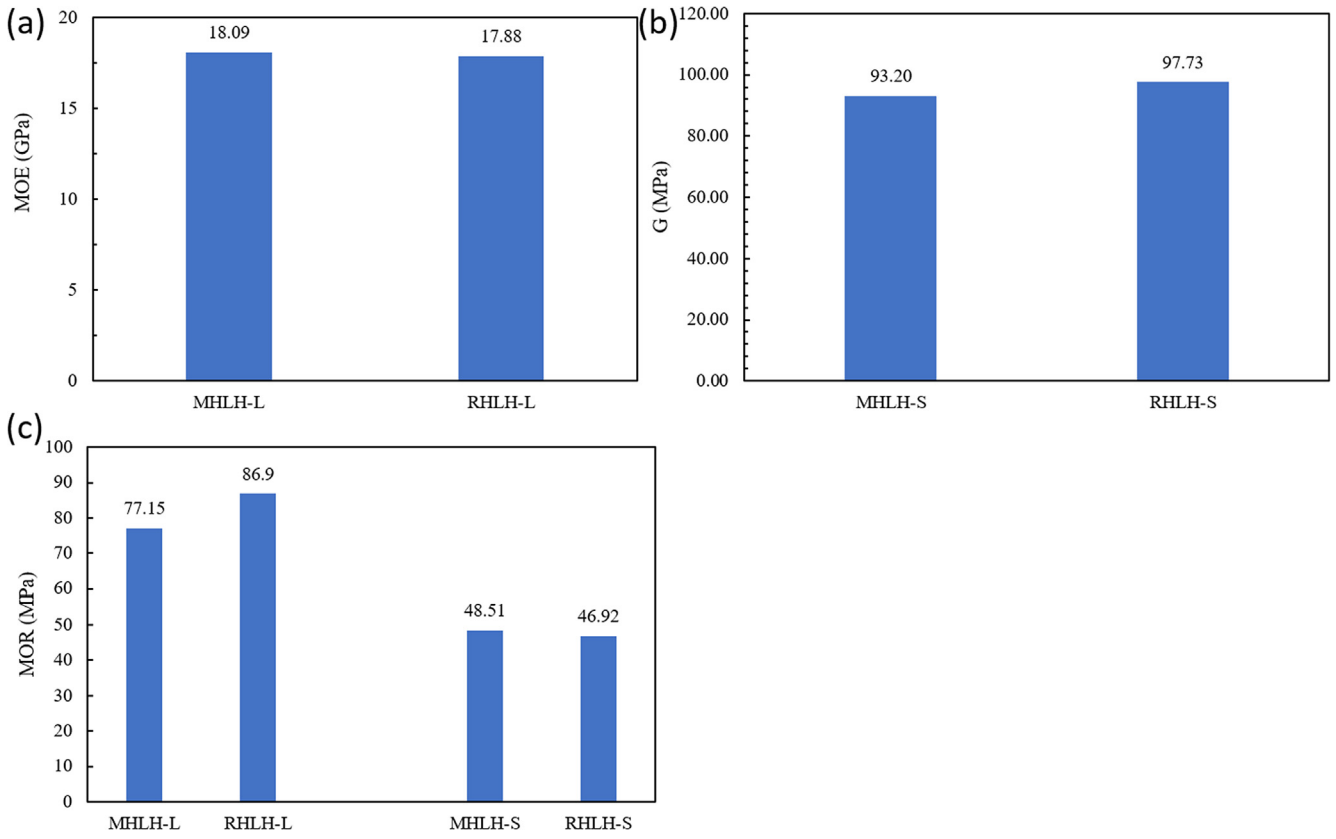

Fig. 5. Bending and shear properties of the CLT beams with different types of adhesives. (a) bending modulus of elasticity (MOE_{CLT}); (b) shear modulus (G); (c) bending modulus of rupture ($MOR_{CLT\text{-}L}$ and $MOR_{CLT\text{-}S}$).

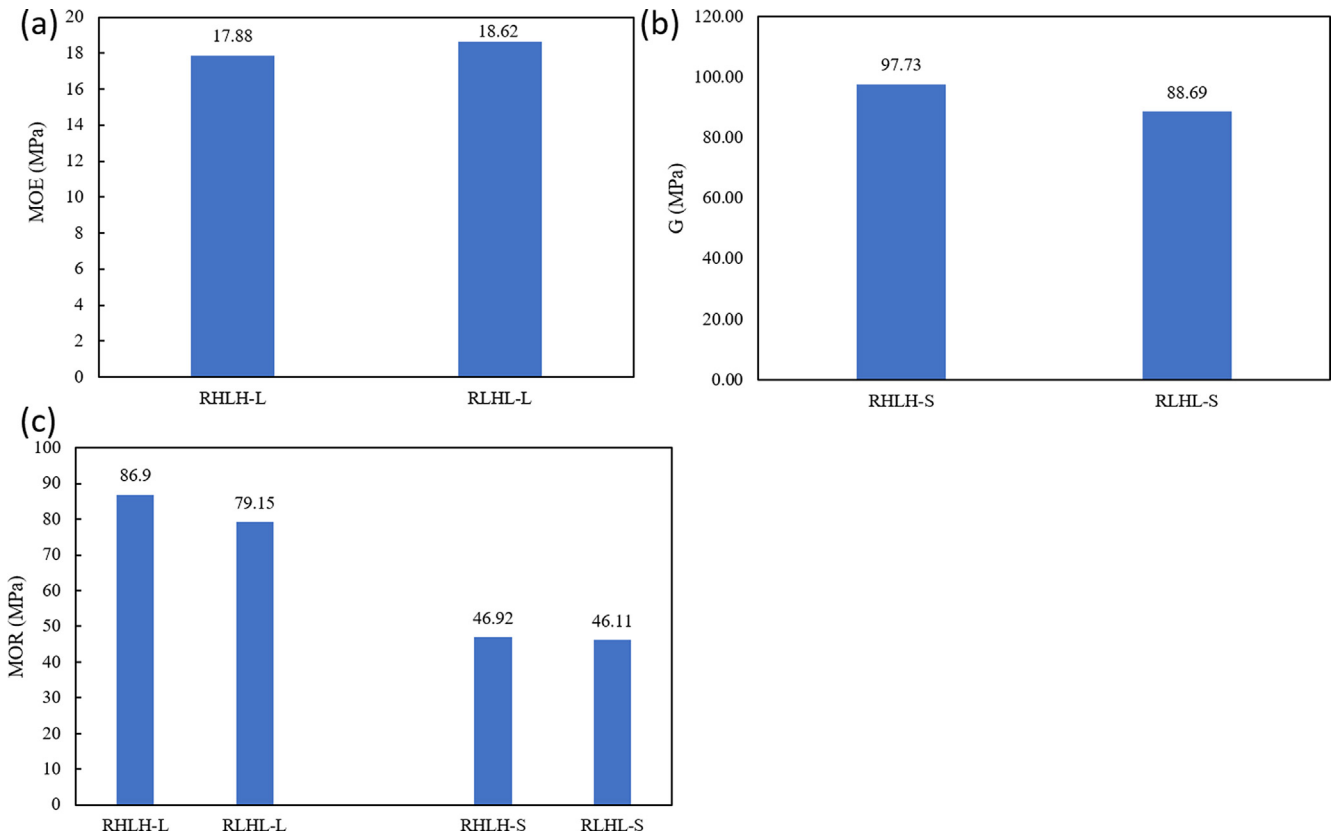

Fig. 6. Bending and shear properties of the CLT beams with different layups. (a) bending modulus of elasticity (MOE_{CLT}); (b) shear modulus (G); (c) bending modulus of rupture ($MOR_{CLT\text{-}L}$).

which reached 9.8%. It indicates that the bending strength is effectively improved when using higher grade lumber in outer layers. The shear strength of the CLT panels was not obviously (1.7%) affected by the different layups in this study. The reduction of differences in the short-span flexural behavior illustrated that the grade of middle layer could have higher impact than the outer layers grade.

4.6. Comparison with the reference values in APA/PRG-320

The design properties for CLT with different grades and layups are provided in the standard for performance-rated Cross-Laminated-Timber ANSI/APA PRG 320 [3]. According to the standard, the CLT panels with E1 grade shows the best performance. The three-layer E1 CLT panel is composed of two longitudinal outer layers made by 1950f-1.7E spruce-pine-fir MSR lumber and one middle layer made by No.3 Spruce-pine-fir lumber as the transverse layer. The comparison of MOE between the reference value in APA/PRG-320 and the experimentally measured value is shown in Fig. 7. The short-span test contains the shear effect and the deformation of the fixtures. As a result, only the tested MOE_{CLT} of the long-span CLT panel is used to represent the MOE_{CLT} of the tested CLT panel types in this study. It can be seen from Fig. 7 that all the manufactured CLT samples with different types of adhesives and layups are providing a higher MOE_{CLT} than the designed value for the highest grade (E1) CLT panel provided in the standard [3]. The MOE_{CLT} of the CLT panels have been improved around 50% to 80% compared to the reference value in the standard [3].

The comparison of MOR_{CLT} between the reference value in APA/PRG-320 and the tested value of the samples is shown in Fig. 8. The MOR_{CLT} of the different types of CLT panel samples was at least two times higher than that of reference value for the E1 CLT [3]. It indicates that the strength was improved vastly when the low-value sugar maple was utilized in CLT panels comparing with standard layup requirement. The results illustrate that both MOE_{CLT} (Fig. 7) and MOR_{CLT} (Fig. 8) of the CLT manufactured in this study

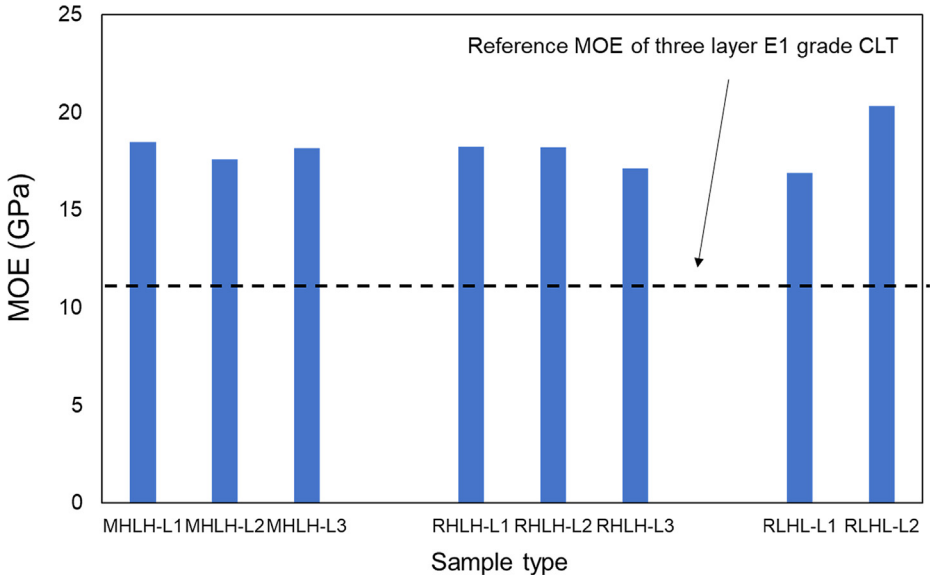

Fig. 7. Comparison of MOE_{CLT} between the reference value in APA/PRG-320 [3] and the tested value.

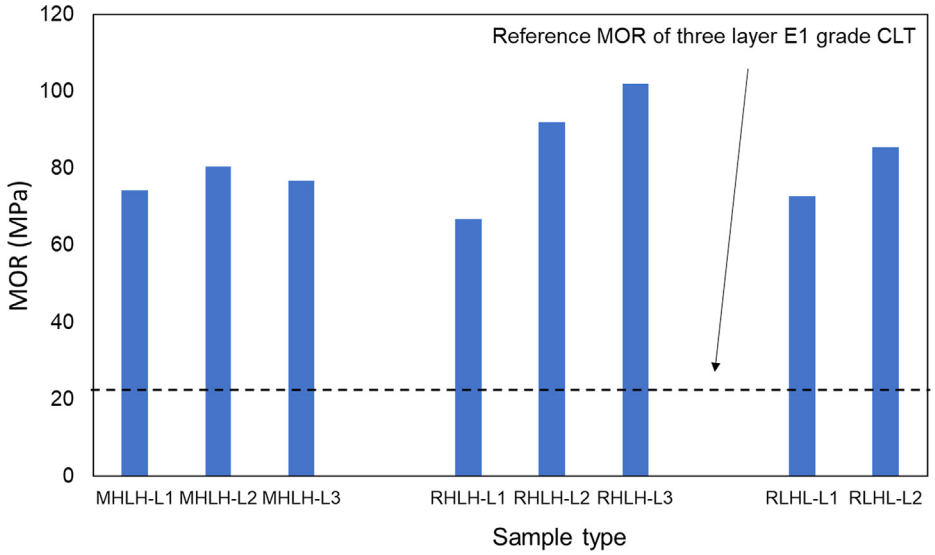

Fig. 8. Comparison of MOR_{CLT} between the reference value in APA/PRG-320 [3] and the tested value.

present a higher value than the reference value of the E1 CLT panels. It indicates that the low-value sugar maple can provide adequate mechanical strength for future manufacture of the CLT panels.

4.7. Comparison with reference values of CLT made with some other species

The tested MOE and MOR of the sugar maple CLT panels along with some reference values of CLT panels made with other species are listed in Table 4. Since the shear modulus and strength are not available in some of the reference, only the bending properties are presented here for comparison. The presented reference values are the highest of their group in the related literatures. The tested sugar maple CLT panels provided 25% to 102% higher MOE than the reference values of CLT samples made with other species, including hardwood as high-quality Yellow Poplar and Oriental oak. The reference MOR of the hardwood species CLT may contain some mistake. When comparing with the reference softwood CLT, the MOR of the tested sample were 2.29–4.35 times as the reference values. The results illustrated that the sample CLT panels made with low-value sugar maple lumber have a higher bending stiffness and strength. The superior mechanical properties of the sugar maple lumber would be the primary reason for the improvement.

5. CLT panel constitutive model and damage model

5.1. Material constitutive model

To study the panel bending and shear performance in the long span test and short span test, finite element software ABAQUS [34] with orthotropic material and damage model was used to provide an additional point of view. The timber material is homogenized with the average properties to avoid the requirement of detailed modeling with grain, growth ring, and knots. Numerous parameters and uncertainties such as the grain direction, knots, checks, as well as the current moisture content distribution, lead to high variation in timber material properties. Though it may lack some of the features, the simplification of material model can reduce the computational cost while providing reasonable estimation for design and construction purposes. The moisture content (MC) of the timber material is also assumed to be constant at 12%.

Table 4
Comparison of MOE and MOR with CLT made with some other species.

Layup or species	MOE (GPa)	MOR (MPa)
MHLH	18.09	77.15
RHLH	17.88	86.90
RLHL	18.62	79.15
Southern pine [15]	9.20	19.98
Irish Sitka spruce [31]	12.24	33.62
Canadian hemlock [14]	11.67	22.40
Oriental oak [32]	13.90	–
Yellow poplar (high quality) [33]	14.23	9.01

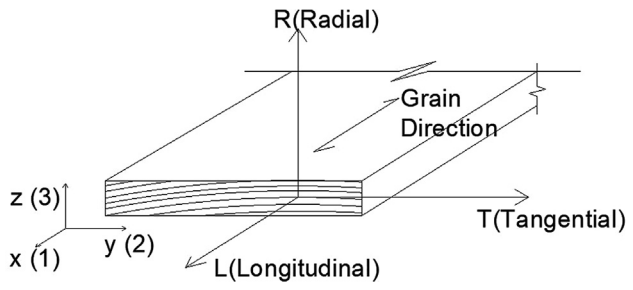

Fig. 9. Principal axes and direction scheme for lamination in major strength direction.

With 1, 2 and 3 separately representing x, y, and z directions, the homogenous orthotropic elastic material model is used to simulate the CLT laminations, as shown in Fig. 9. The elastic compliance of the material is set as Eq. (7).

$$\begin{Bmatrix} \sigma_{11} \\ \sigma_{22} \\ \sigma_{33} \\ \gamma_{12} \\ \gamma_{13} \\ \gamma_{23} \end{Bmatrix} = \begin{bmatrix} 1/E_1 & -v_{21}/E_2 & -v_{31}/E_2 & 0 & 0 & 0 \\ -v_{12}/E_2 & 1/E_2 & -v_{32}/E_2 & 0 & 0 & 0 \\ -v_{13}/E_2 & -v_{23}/E_2 & 1/E_3 & 0 & 0 & 0 \\ 0 & 0 & 0 & 1/G_{12} & 0 & 0 \\ 0 & 0 & 0 & 0 & 1/G_{13} & 0 \\ 0 & 0 & 0 & 0 & 0 & 1/G_{23} \end{bmatrix} \times \begin{Bmatrix} \sigma_{11} \\ \sigma_{22} \\ \sigma_{33} \\ \sigma_{12} \\ \sigma_{13} \\ \sigma_{23} \end{Bmatrix} \tag{7}$$

where $\varepsilon_{ii}$and $\gamma_{ij}$are the strain of the corresponding directions, E_i is the elastic moduli in each direction, v_{ij} is the Poisson's ratio of direction i and j, G_{ij} is the shear modulus between direction i and j, and σ_{ij} is the corresponding stress. As $v_{ij}/E_i = v_{ji}/E_j$, nine parameters including three elastic modulus E_1, E_2 and E_3, three shear modulus G_{12}, G_{13} and G_{23} and three Poisson's ratios v_{12}, v_{13} and v_{23} are required to be input in the material model

5.2. Constitutive model parameters

The model is input with mechanical properties of each layer based on the reference data provided in Wood Handbook [35] and the average value of nondestructive vibration flexural test of laminations from Table 1. In Wood Handbook [35], the elastic modulus in tangential and radius direction and shear modulus in longitudinal-radius and longitudinal-tangential directions are provided as 0.065, 0.132, 0.111 and 0.063 of the longitudinal elastic modulus, respectively. Note that the ratio of G_{RT}/E_L is not available for sugar maple. It is assumed based on data of yellow poplar, which is also a diffuse-porous hardwood and have similar specific gravity range as sugar maple, according to the Wood Handbook [35] as 0.011. In a study by Dickinson et al. [12], the average longitudinal elastic modulus of sugar maple was found as 13.3 GPa, which is close to the measured value. In another study by Gong et al. [36], the planar shear modulus (G_{RT}) of white and yellow birch, which are also diffuse-porous hardwood, varies from 161 MPa to 193 MPa, which is close to the assumed value.

Then for each layer of laminations, the elastic modulus in other directions and shear modulus are calculated based on provided converting ratio and the reference elastic modulus of grain direction. For longitudinal layers of the CLT sample, the properties in direction L, T, and R are separately inputted as in directions 1, 2, and 3 in Eq. (7). As the grain direction is perpendicular to the major strength direction, the transverse layer is defined as the properties in direction L, T, and R separately in the direction of 2, 1, and 3. The input elastic modulus and shear modulus are as shown in Table 5. The Poisson's ratios are considered only depending on the species, which are provided by Wood Handbook [35]. The v_{12}, v_{13} and v_{23} of the longitudinal layers are separately 0.476, 0.424 and 0.349 while for the transverse layers, they are 0.037, 0.349 and 0.424, respectively.

Table 5
Elastic modulus and shear modulus input of each layer (Unit: MPa).

Layer type		E_1	E_2	E_3	G_{12}	G_{13}	G_{23}
MHLH (1L-3L, 1S1-3S4)	longitudinal layers	1.75×10^4	1.13×10^3	2.30×10^3	1.94×10^3	1.10×10^3	1.92×10^2
	transverse layer	4.71×10^2	9.56×10^2	7.24×10^3	7.97×10^1	4.56×10^2	8.04×10^2
RHLH (1L-3L, 1S1-3S4)	longitudinal layers	1.65×10^4	1.08×10^3	2.18×10^3	1.84×10^3	1.04×10^3	1.82×10^2
	transverse layer	6.48×10^2	1.32×10^3	9.97×10^3	1.10×10^2	6.28×10^2	1.11×10^3
RLHL (1L-2L, 1S1-2S4)	longitudinal layers	9.07×10^3	5.90×10^2	1.20×10^3	1.01×10^3	5.72×10^2	9.98×10^1
	transverse layer	1.33×10^3	2.70×10^3	2.04×10^4	2.25×10^2	1.29×10^3	2.27×10^3

5.3. Progressive damage model

To capture the damage behavior of orthotropic material as timber, the progressive damage analysis model applied is a generalized approach proposed by Camanbo and Davila [37]. The process combines linearly elastic behavior of the undamaged material with the Hashin's damage initiation criteria [23], and the damage evolution model follows a linear pattern with the defined fracture energy for each damage modes.

The initiation of damage is detected by the Hashin and Rotem damage criteria regarding nominal Cauchy stresses σ, which is computed by the finite-element analysis procedures [38]. The onset of degradation at a material point is referred to as damage initiation. The timber material is considered as a composite of fiber and matrix. In the longitudinal direction, the equilibrium matrix and fiber will contribute as a combination, while for the transverse direction, only the matrix is considered working. The Hashin's criteria consider four different damage mechanisms. As shown in Eqs. (8)–(11), the four indexes defining the damage criteria are the tensile along the fiber direction F_f^t, the compressive along the fiber direction F_f^c, the transverse tensile F_m^t, and transverse compressive F_m^c.

(1) Longitudinal tension: fiber tension ($\sigma_{11} \geq 0$)

$$F_f^t = \left(\frac{\sigma_{11}}{F_{1t}}\right)^2 + \alpha\left(\frac{\sigma_{12}}{F_6}\right)^2 \tag{8}$$

(2) Longitudinal compression: fiber compression ($\sigma_{11} \leq 0$)

$$F_f^c = \left(\frac{\sigma_{11}}{F_{1c}}\right)^2 \tag{9}$$

(3) Transverse tension and/or shear: matrix tension and/or shear ($\sigma_{22} \geq 0$)

$$F_m^t = \left(\frac{\sigma_{22}}{F_{2t}}\right)^2 + \left(\frac{\sigma_{12}}{F_6}\right)^2 \tag{10}$$

(4) Transverse compression: matrix compression ($\sigma_{22} < 0$)

$$F_m^c = \left(\frac{\sigma_{22}}{2F_4}\right)^2 + \left[\left(\frac{F_{2c}}{2F_4}\right)^2 - 1\right]\frac{\sigma_{22}}{F_{2c}} + \left(\frac{\sigma_{12}}{F_6}\right)^2 \tag{11}$$

where σ_{ij} are the components of the stress tensor, and α determines the contribution of the shear stress to the fiber tensile criterion. F_{1t}, F_{1c}, are the tensile and compressive strengths in the longitudinal direction; F_{2t}, F_{2c}, are the tensile and compressive strengths in the matrix direction; F_6, F_4 are the longitudinal and transverse shear strengths. Damage initiation occurs when any of these indexes reaches 1.0. The simulation will be automatically stopped when the damage occurs. As timber is a brittle material, the model was capable to capture the material failure and damage initiation. The calculated contours of the four damage indexes would provide an estimation of the damage initiation location.

5.4. Damage model parameters

To simulate the material damage, the strengths are assigned in the longitudinal and transverse directions to each layer accordingly. The strengths of each layer are calculated based on reference value and the measured lamination MOE. Based on the study of timber strength and MOE correlations [39,40], the strengths of each layer are assumed to be proportional to the reference values by the ratio of the longitudinal elastic modulus to reference MOE of sugar maple. The reference longitudinal compressive strength is 73 MPa (10587 psi) in a dry condition, as studied by Hernandez [41]. The reference longitudinal tensile strength and transverse compressive strength value are provided by Wood Handbook as 108.25 MPa (15700 psi) and 10.13 MPa (1470 psi) respectively. The longitudinal shear strength of sugar maple was tested in a study by Okkonen and River [42] as an average of 15.92 MPa (2309 psi) when using the ASTM D143 block shear method. According to the Wood Handbook, the transverse shear strength can be estimated as 18–28% of longitudinal shear strength [35]. Accordingly, the estimated strengths of layers in each group are calculated and listed in Table 6. As in the material model parameter section, for longitudinal layers, the strengths in longitudinal directions are input as F_{1c}, $F_{1t}$and F_6, the transverse direction strengths are considered as F_{2c}, F_{2t} and F_4. While for the transverse layers, the input order is reversed. The longitudinal strengths of the lumber are input as F_{2c}, F_{2t} and F_4, and the transverse strengths as F_{1c}, F_{1t} and F_6 respectively.

6. Finite element simulation of panel test and comparison of simulation results with test data

6.1. Simulation of long-span CLT panel flexural test

6.1.1. Finite element modeling of long-span CLT panel flexural test

The model geometry and boundary conditions were established based on the test program. The schemes of the long span test sim-

Table 6
Strengths properties of each layer in the model (unit: MPa).

Layer type		F_{1c}	F_{1t}	F_{2c}	F_{2t}	F_6	F_4
MHLH-(L1-3, S1-6)	longitudinal layers	1.46×10^4	2.17×10^4	2.03×10^3	1.10×10^3	3.19×10^3	7.34×10^2
	transverse layer	8.44×10^2	4.56×10^2	6.08×10^3	9.01×10^3	3.05×10^2	1.32×10^3
RHLH-(L1-3, S1-6)	longitudinal layers	1.39×10^4	2.06×10^4	1.93×10^3	1.04×10^3	3.03×10^3	6.96×10^2
	transverse layer	1.16×10^3	6.28×10^2	8.37×10^3	1.24×10^4	4.19×10^2	1.82×10^3
RLHL-(L1,L2,S1-6)	longitudinal layers	7.61×10^3	1.13×10^4	1.06×10^3	5.72×10^2	1.66×10^3	3.82×10^2
	transverse layer	2.38×10^3	1.29×10^3	1.72×10^4	2.54×10^4	8.60×10^2	3.74×10^3

ulation follow the test configurations, as shown in Fig. 2. The panel model was evenly meshed to three-dimensional solid element with the mesh size of 5 mm. The meshing size was determined in a series of parametric convergency study of the MHLH model. The loads were applied with controlled displacements at surface nodes. The left supports were assigned as restrained in all three directions, while the right support was only restrained in the vertical and transverse direction. Then the sample was set as vertically supported and allowed for the rotation and longitudinal sliding as in the experimental test.

The timber layers were assigned with the material constitutive and damage model according to the layer location. The top and bottom layer were separately assigned with the parameters of the longitudinal layers as shown in the Table 5, while the middle layers were assigned as the transverse layer. The material properties parameters were generated with the directions. Similarly, the strengths of each layer were input as the damage criteria as in Table 6 for the damage model to determine the occurrence of damage. Since the load was applied with controlled displacement, the sum of vertical reaction on the loading points were recorded as

Table 7
Simulated results of the long-span tests and comparison.

CLT type	Peak load (kN)	Displacement at peak load (mm)	MOE_{CLT} (GPa)	MOE_{CLT} difference with the tested average	MOE_{CLT} difference with shear analogy analysis value	MOR_{CLT-L} (MPa)	MOR_{CLT-L} difference with the tested average
MHLH	53.50	90.00	15.40	11.50%	5.95%	85.40	10.70%
RHLH	59.20	102.00	15.00	12.90%	31.43%	94.40	8.60%
RLHL	47.70	143.00	8.65	−37.70%	10.57%	76.10	−4.00%

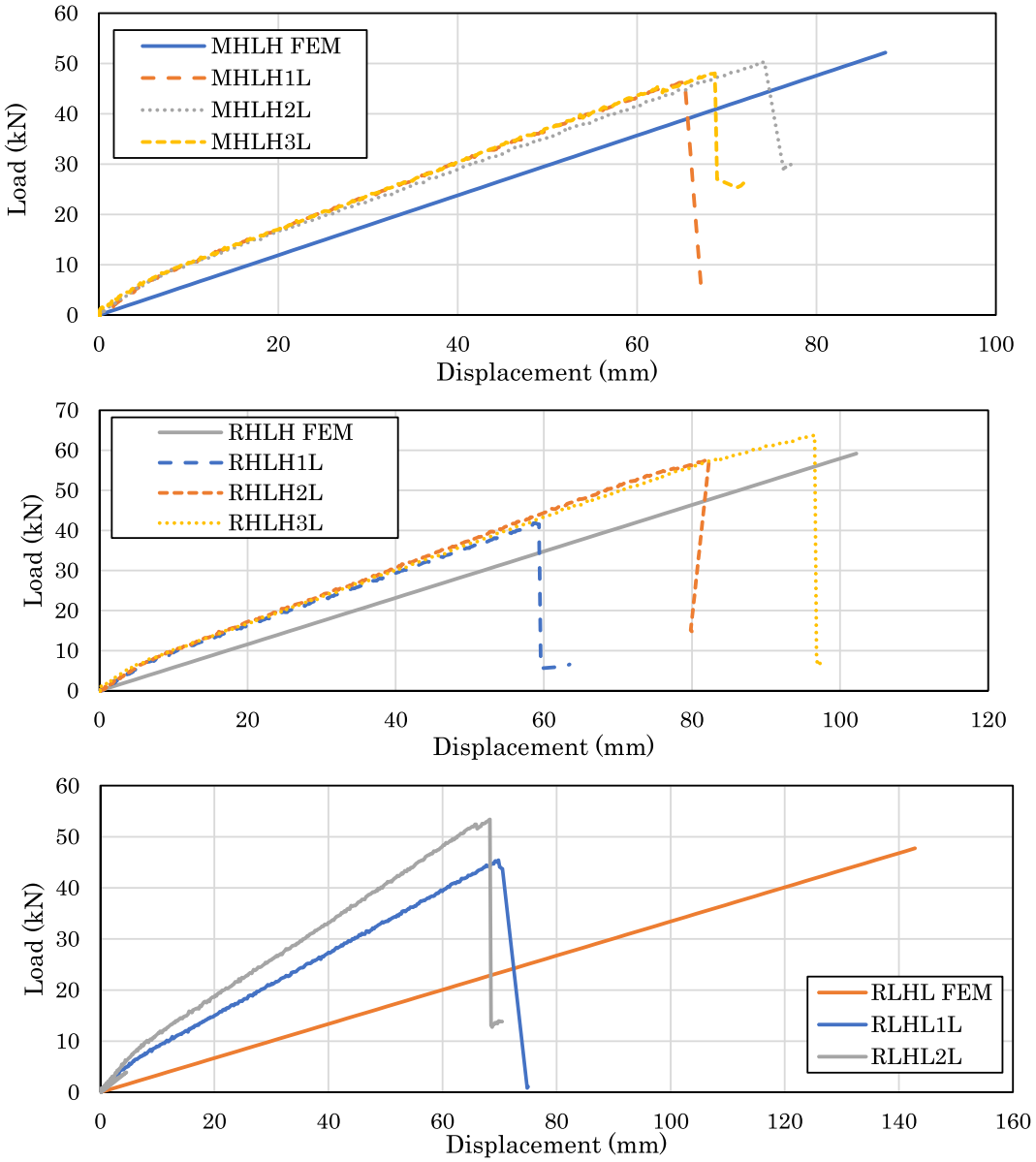

Fig. 10. Load-displacement curves of the simulated and experimental long span tests (a) Type MLHL; (b) Type RHLH; (c) Type RLHL.

the total load. The vertical displacements of the center bottom nodes were recorded as the mid-span displacement.

6.1.2. Comparison of simulation results and test result of long-span tests

With the model input, the simulations of the long-span tests were able to provide an estimation of the sample failures. The damage model provided an estimation of the damage occurrence, which was a compressive damage on the top layer in between the loading points. It could be the underestimation of the compression parameter that caused the error of damage mode estimation. The local defects including knots and wane were also not considered, which limited the ability of the model to detailly predict the damage occurrence location. It could also be the result of the overestimation of the transverse shear strength parameter. The simulated peak load and displacement of all three CLT types were listed in Table 7. The MOE and MOR were calculated accordingly following Section 3.2. The simulated load–displacement curve of the MHLH panel in the long-span test is as shown in Fig. 10 (a).

The peak load is 53.54 kN at the displacement of 89.99 mm, which agrees with the tested results range as shown in Table 2. The simulated bending elastic modulus (MOE_{CLT}) is 15396 MPa, which is 11.5% higher than the average test result and 7.7% higher than the sample with the highest tested result. The estimated modulus of elasticity (MOE_{CLT}) can be considered as an adequate estimation of the tests. The simulated $MOR_{CLT\text{-}L}$ has a difference of 10.7%, which is also within the range of tested results. Similarly, as shown in Fig. 10 (b), for RHLH CLT type, the modeled results are also close to the average and the range of test results, which are 12.9% higher in elastic modulus and 8.6% higher in bending strength. However, for the RLHL case, as shown in Fig. 10 (c), the simulated MOE_{CLT} has a relatively large difference to the tested results. The simulated MOE_{CLT} is 37.7% less than the average. The reason might be that the actual MOE_{CLT} of the lamination was much higher than the tested value. On the contrary, the calculated $MOR_{CLT\text{-}L}$ was still providing an adequate estimation, which is 4% less than the average and in between the tested result. The MOE was also estimated with the shear analogy analysis according to the CLT handbook [30]. The MOE for MHLH from shear analogy analysis were close with the test results. The shear analogy analysis provided an overestimation for the MOE for RHLH. For the RLHL, however, the MOE calculated with shear analogy method is closer to the simulation result, which contains about 20 percent of underestimation comparing to the test results. The major cause of the error except the variance of lumber might be the error contained in the estimated lumber modulus parameters, especially in the transverse direction. The convert factors could be improved with more mechanical tests of the certain species and source region of lumber.

6.2. Simulation of Short-span CLT panel flexural test

6.2.1. Finite element modeling of Short-span CLT panel flexural test

As shown in Fig. 3 (a), the sample rests on two support bars on a channel beam and loaded by the loading head during the test. As the measured displacement contains the elastic deformation of fixtures, the calibration of beam deformation by deducting the elastic deformation was first conducted with the simulation of a model of

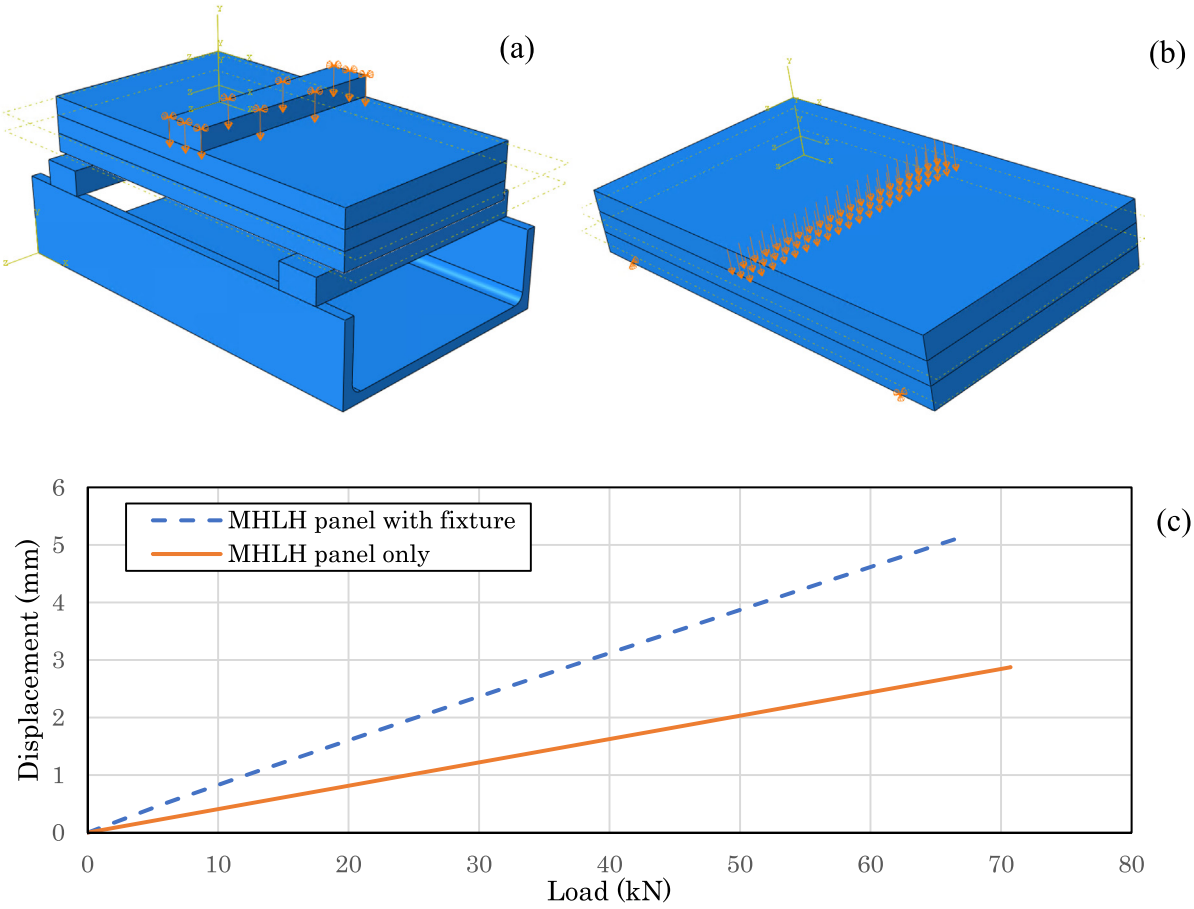

Fig. 11. Simulation of the short-span test models and results for displacement calibration (a) model of a panel with fixture, (b) model of a panel only, and (c) result comparison of models with and without the fixture.

only the sample (Fig. 11(b)) and another model with the fixture and sample (Fig. 11(a)).

The support and loading heads are simulated as isotropic elastic metal parts. The three-layer MHLH sample is placed on two supporting bars and is loaded with a loading head in mid-span. The supporting bars are resting on the channel base. The channel base is supported by around hydraulic jack head. Except for the supporting bars, all parts are made with the exact dimensions. The supporting bars were substituted with rectangular bars considering the potential difficulty of surface contact convergency. As the support bars are subjected to bending, and the self-weight is negligible compared with the applied loads, they can be substituted with bars with the equivalent moment of inertia. The original support bars contain a hollow circular tube (inner diameter 38.1 mm, outer diameter 50.8 mm) at the bottom and 6.35 mm thick, 50.8 mm wide plate at the top. Two rectangular bars with 50.8 mm width and 31.75 mm depth is modeled to represent the original supporting bars.

The loading head is assigned as the type 7000 aluminum alloy, which has an elastic modulus of 68.95 GPa and a Poisson's ratio of 0.33. The support bar and the channel base models are assigned with an elastic modulus of 77.91 GPa and a Poisson's ratio of 0.26 as A36 low carbon steel. As the measurement of displacement was relative to the jack head, the bottom support was considered as very stiff material, with an elastic modulus of one million GPa. The CLT sample was assigned to the previous MHLH type properties. All contacts were assigned as hard contact in normal direction and friction coefficient of 1.0 in the tangential direction. The established model is as shown in Fig. 11 (a). Meanwhile, a model of only the panel was established based on Fig. 3 (b) as shown in Fig. 11 (b)

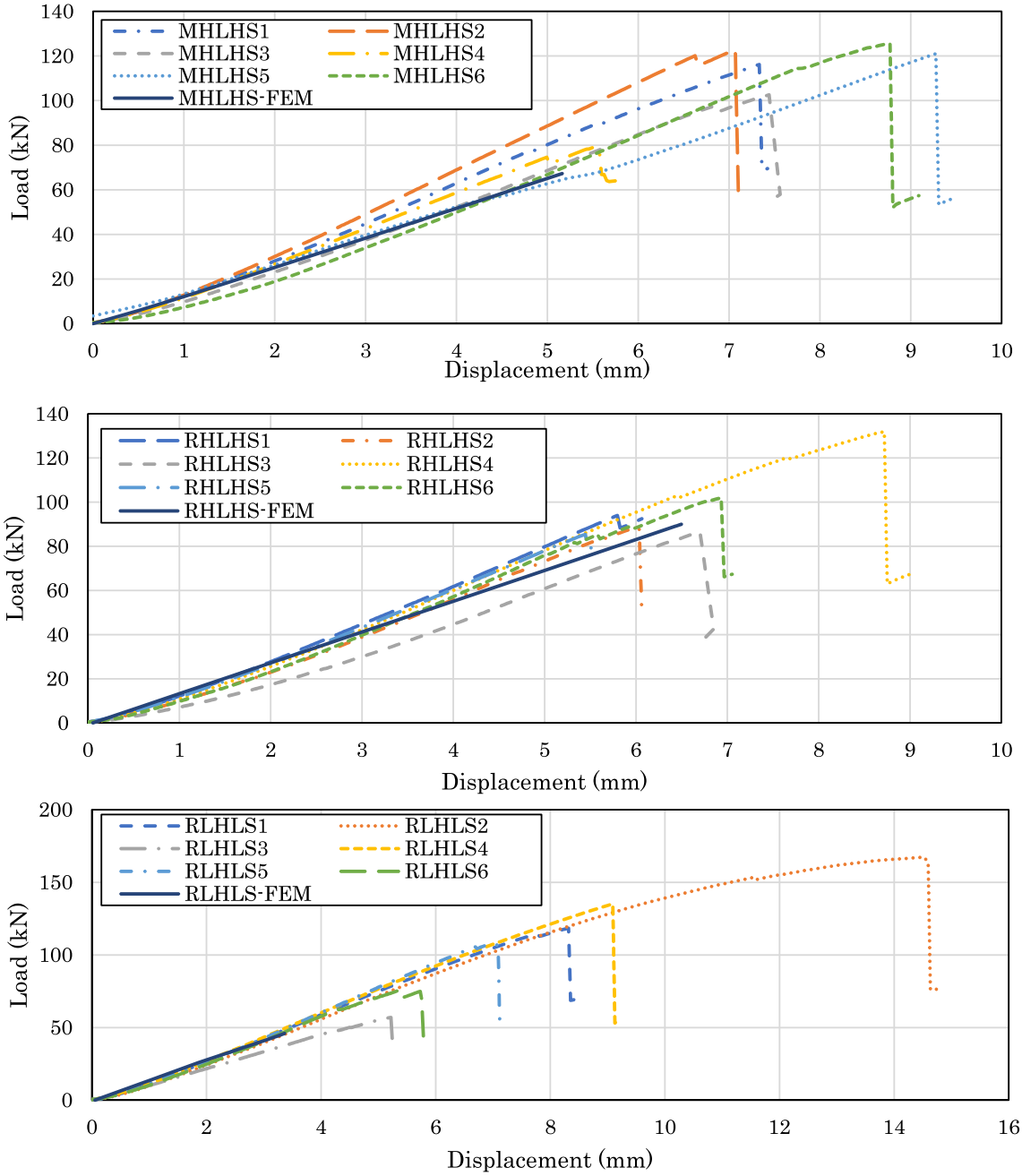

Fig. 12. Simulated and tested results of short span samples (a) Type MHLH (b) Type RHLH (c) Type RLHL.

with the stiffness parameters of MHLH type as listed in Table 5. Similar with the long-span model, the model was meshed to C3D8R brick element. The meshing size was 5 mm. For the sample with fixture model, the bottom rigid plate was fixed and support the channel beam. For the sample only model, the left supports were restrained in all three directions while the right supports were restrained in vertical and transverse direction. The load were applied with controlled displacement in both of the models.

The simulated load–displacement curves are shown in Fig. 11 (c). The relative displacement caused by the sample is around 0.53 of the combined one with both the fixtures and the sample. As the fixture is designed to stay in elastic behavior during the test, the load–displacement correlation of the caused by the fixture can be estimated as the linear difference between the results of beam only model and beam with fixture model. Based on the Fig. 11 (c), for each 10 kN applied onto the sample, the fixture deforms 0.35 mm.

6.2.2. Comparison of simulation results and test result of short-span tests

Based on the calculated fixture load–displacement correlations and the sample models, the simulated load–displacement curves of MHLH-S, RHLH-S, and RLHL-S panels are shown in Fig. 12 (a), (b) and (c) respectively. The damage model results indicated the damage initiated in the center layer around third points, which is in good agreement with the test results. Since the bonding and the defects of the lumber were not considered, the detailed damage location was not able to be estimated. The simulated peak loads and correlated displacement are listed in Table 8. The shear modulus and equivalent MOR were calculated as in Section 3.3. These simulation results were compared with the correlated tested results. As shown in Fig. 11, the estimated shear modulus G (as listed in Table 8) are having a steady difference to the average tested values, as the different percentages varies from 22.76% to 27.96%. Meanwhile, for the $MOR_{CLT\text{-}S}$, only the RHLH sample can provide a relatively close estimation. The simulated $MOR_{CLT\text{-}S}$ of sample type MHLH and RLHL are separately 34% and 52.3% less than the group average from the tests. To be noticed, the $MOR_{CLT\text{-}S}$ vary in a large range for the tests, as shown in Table 3. The range of MHLH $MOR_{CLT\text{-}S}$ is 57% relative to the weakest sample in the group, while it is 132% for RLHL group. For both the sample types, the simulated results are less than (up to 25%) the values of the weakest sample. It indicates that the lumber strength parameter estimation is conservative under these cases. The results can be considered as a close conservative estimation of the tests as the tested data contains high variations. Similarly, the results of the short span tests were also estimated with the shear analogy analysis according to the CLT handbook, as shown in Table 8. When comparing with the result of shear analogy analysis, the shear modulus from simulation were 30–74% smaller. The result indicate that the shear analogy overestimated the shear modulus, especially for the LHL layup. The first cause could be the overestimation contained the shear influence factor, as the experiment setting of the sample was not an ideal simply supported beam. It is also observed that higher modulus in the middle layer could increase the overestimation of the shear analogy analysis and FEA. The reason could be the same as in the long-span test, which is the limitation in the convert factors of the lumber modulus and the assumption of ideal linear correlation.

7. Conclusion

In this study, we evaluated the mechanical properties of CLT panels made from low-value sugar maple with integrated long-span and short-span bending tests and finite element model simulation. By sorting the laminations to High and Low groups, three types of CLT beams were designed and evaluated, including Melamine "High-Low-High" (MHLH), Resorcinol "High-Low-High" (RHLH) and Resorcinol "Low-High-Low" (RLHL). Both long-span and short-span bending tests were conducted on the CLT specimens to obtain the flexural and shear properties according to the ASTM D198. By applying the orthogonal constitutive and progressive damage model along with the calibrated model parameters, the beam flexural and shear stiffness and strength were predicted with finite element simulation. The following conclusions can be drawn from this study.

1. The wood failure percentage was over 85% in the block shear tests for all the three groups of samples, which indicated the bonding quality can be considered adequate. The bonding shear strength for Melamine bonded sugar maple samples was 4.7 MPa, which is higher than Resorcinol bonded ones.
2. In the long-span bending test, the Resorcinol glued samples have 12.6% more bending strength compared to Melamine glued samples, while the stiffness were close. The CLT samples with HLH layup presented an improved bending strength which is 9.8% higher than the result of LHL group. The difference in layups caused minor difference (4%) on the MOE. It demonstrated that the major direction bending strength of CLT could be improved by applying higher quality lumber in outer layers, while the modulus may not be influenced much.
3. Based on the short span bending test results, the adhesive type did not have obvious impact on the shear modulus and shear strength (1%). The short span test results of the HLH samples showed 6.7% higher in shear modulus and 1.7% in shear strength comparing with the LHL samples. These differences illustrated that the quality of middle layer could contribute more than the outer layers in the short-span flexural behavior.
4. The low-value sugar maple CLT samples provided higher mechanical properties compared with the current standard E1 layups in APA/PRG-320. Specifically, the bending MOE of the sugar maple CLT increased about 50% to 80% comparing to the reference value of layup E1. The bending strength values of the sugar maple CLT of all three layups were at least five times the values of the standard layup E1 in APA/PRG-320. The results were also compared with the reference value of CLT panels made with other species from literature. The MOE of the low-value sugar maple samples were 25% to 102% higher than the reference values and the MOR were 2.29–4.35 times as the reference values.
5. The simulated results indicate that the model can provide a close estimation of the flexural properties of the CLT panels,

Table 8
Simulated results of the short span tests and comparison.

Sample type	Peak load (kN)	Peak displacement (mm)	G (MPa)	G difference with the average test value	G difference with shear analogy analysis value	$MOR_{CLT\text{-}S}$ (MPa)	$MOR_{CLT\text{-}S}$ difference with the average test value
MHLH	67.3	5.16	71.11	−23.70%	−30.33%	32.2	−34%
RHLH	90	6.5	75.49	−22.76%	−45.45%	43	−8.30%
RLHL	45.9	3.35	63.9	−27.96%	−73.95%	22	−52.30%

including MOE, MOR and shear modulus. The simulation results were in good agreement with the experimental results with minor reasonable difference. For long-span tests, the relative difference in bending elastic modulus was less than 13% for both MHLH and RHLH types, while it was 37.7% for RLHL type. The reason could be the conservativeness in material parameter determination. The simulated bending strength have less than 10.7% of relative difference for all three types of CLT. For short-span tests, the simulation resulted in a relative steady underestimation of shear modulus (22.8% to 28.0%) comparing with the average measured values. Since the test results exhibited a large variation, the simulation results are considered as a conservative estimation.

In summary, the bending and shear stiffness and strength of lab-manufactured low-value sugar maple CLT panels are improved by comparing with current standardized softwood CLT and reference values of other species. The developed finite element model with calibrated model parameters was able to provide a reasonable estimation of the bending and shear properties of the CLT samples. The integrated experimental and computational tools can reveal the flexural damage behavior of CLT panels made from low-value sugar maple.

CRediT authorship contribution statement

Yunxiang Ma: Methodology, Software, Formal analysis, Investigation, Data curation, Writing - original draft, Writing - review & editing. **Munkaila Musah:** Investigation, Data curation, Writing - review & editing. **Ruizhe Si:** Formal analysis, Writing - original draft. **Qingli Dai:** Conceptualization, Writing - original draft, Writing - review & editing, Supervision. **Xinfeng Xie:** Conceptualization, Resources, Writing - review & editing, Supervision, Funding acquisition. **Xiping Wang:** Writing - review & editing, Project administration. **Robert J. Ross:** Project administration.

Declaration of Competing Interest

The authors declare that they have no known competing financial interests or personal relationships that could have appeared to influence the work reported in this paper.

Acknowledgements

This study was conducted through a cooperative research agreement (FS 17-JV-11111133-034) between Michigan Technological University and USDA Forest Service and was partially funded by USDA Forest Service, Forest Products Laboratory. The authors also thank AJD Forest Products, L.P. (Grayling, MI), for donating the materials for this project.

References

[1] E. Karacabeyli, B. Douglas, Cross-laminated Timber Handbook US Edition, Special Publications SP-529E: FPInnovations, Pointe-Claire, Quebec, Canada, 2013.
[2] R. Brandner, G. Flatscher, A. Ringhofer, G. Schickhofer, A. Thiel, Cross laminated timber (CLT): overview and development, Eur. J. Wood Wood Prod. 74 (3) (2016) 331–351.
[3] APA, Standard for performance-rated cross laminated timber, ANSI/APA PRG-320-2019, Tacoma, WA, 2019.
[4] X. Sun, M. He, Z. Li, Novel engineered wood and bamboo composites for structural applications: State-of-art of manufacturing technology and mechanical performance evaluation, Constr. Build. Mater. 249 (2020) 118751.
[5] T. Ehrhart, R. Brandner, G. Schickhofer, A. Frangi, Rolling shear properties of some European timber species with focus on cross laminated timber (CLT): test configuration and parameter study, International Network on Timber Engineering Research: Proceedings of Meeting 48, Timber Scientific Publishing, KIT Holzbau und Baukonstruktionen, 2015, pp. 61-76.
[6] T. Ehrhart, R. Brandner, Rolling shear: Test configurations and properties of some European soft-and hardwood species, Eng. Struct. 172 (2018) 554–572.
[7] R.E. Thomas, U. Buehlmann, Using low-grade hardwoods for CLT production: a yield analysis, in: V. Möttönen, E. Heinonen (Eds.), Proceedings of the 6th international scientific conference on hardwood processing; 2017 September 25-28; Lahti, Finland. Helsinki, Findland: Natural Resources Institute of Finland: 199-206., 2017, pp. 199-206.
[8] D. Hovanec, Effect of wood characteristics on adhesive bond quality of yellow-poplar for use in cross-laminated timbers, Department of Wood Science and Technology, West Virginia University, 2015.
[9] M. Mohamadzadeh, D. Hindman, Mechanical performance of yellow-poplar cross laminated timber, Virginia Polytechnic, Institute and State University, 2015.
[10] G. Jeitler, M. Augustin, G. Schickhofer, BIRCH| GLT+ CLT-Mechanical properties of Glued Laminated Timber and Cross Laminated Timber produced with the wood species birch, World Conference on Timber Engineering, Technische Universität Wien, 2016, pp. MS1-07: 2.
[11] S. Franke, Mechanical properties of beech CLT, Proceedings of the WCTE 2016 World Conference on Timber Engineering, Vienna, Austria, 2016, pp. 22-25.
[12] Y. Dickinson, X. Wang, J. Wiedenbeck, R.J. Ross, Effects of silviculture practices on engineering properties of northern hardwood species of the Great Lakes Region: a literature review, Gen. Tech. Rep. FPL-GTR-269. Madison, WI: US Department of Agriculture, Forest Service, Forest Products Laboratory. 17 p. 269 (2019).
[13] ASTM, ASTM D198-15, Standard Test Methods of Static Tests of Lumber in Structural Sizes, ASTM International West Conshohocken, 2015.
[14] M. He, X. Sun, Z. Li, Bending and compressive properties of cross-laminated timber (CLT) panels made from Canadian hemlock, Constr. Build. Mater. 185 (2018) 175–183.
[15] D.P. Hindman, J.C. Bouldin, Mechanical properties of southern pine cross-laminated timber, J. Mater. Civ. Eng. 27 (9) (2015) 04014251.
[16] E.S. Flores, K. Saavedra, J. Hinojosa, Y. Chandra, R. Das, Multi-scale modelling of rolling shear failure in cross-laminated timber structures by homogenisation and cohesive zone models, Int. J. Solids Struct. 81 (2016) 219–232.
[17] R. Brandner, P. Dietsch, J. Dröscher, M. Schulte-Wrede, H. Kreuzinger, M. Sieder, Cross laminated timber (CLT) diaphragms under shear: Test configuration, properties and design, Constr. Build. Mater. 147 (2017) 312–327.
[18] Z. Wang, H. Fu, M. Gong, J. Luo, W. Dong, T. Wang, Y.H. Chui, Planar shear and bending properties of hybrid CLT fabricated with lumber and LVL, Constr. Build. Mater. 151 (2017) 172–177.
[19] R. Brandner, R. Tomasi, T. Moosbrugger, E. Serrano, P. Distch, Properties, Testing and Design of Cross Laminated Timber, A State-Of-The-Art Report by COST Action FP1402/WG2, 2018.
[20] M. Li, Evaluating rolling shear strength properties of cross-laminated timber by short-span bending tests and modified planar shear tests, J. Wood Sci. 63 (4) (2017) 331–337.
[21] S. Navaratnam, P. Christopher, T. Ngo, T. Le, Bending and shear performance of Australian Radiata pine cross-laminated timber, Constr. Build. Mater. 232 (2020) 117215.
[22] Y. Chen, F. Lam, Bending performance of box-based cross-laminated timber systems, J. Struct. Eng. 139 (12) (2013) 04013006.
[23] Z. Hashin, A. Rotem, A fatigue failure criterion for fiber reinforced materials, J. Compos. Mater. 7 (4) (1973) 448–464.
[24] M. Gharib, A. Hassanieh, H. Valipour, M. Bradford, Three-dimensional constitutive modelling of arbitrarily orientated timber based on continuum damage mechanics, Finite Elem. Anal. Des. 135 (2017) 79–90.
[25] B. Brank, A. Stanić, M. Lavrenčič, B. Hudobivnik, Design optimization and failure modelling of ribbed cross-laminated timber plates, Shell Structures: Theory and Applications Volume 4: Proceedings of the 11th International Conference“ Shell Structures: Theory and Applications,(SSTA 2017), October 11-13, 2017, Gdansk, Poland, CRC Press, 2017, p. 69
[26] ASTM, ASTM D6874-12, Standard Test Methods for Nondestructive Evaluation of Wood-Based Flexural Members Using Transverse Vibrations, ASTM International West Conshohocken, 2012.
[27] M. Musah, BONDING HARDWOOD LUMBER FOR CROSS LAMINATED TIMBER: PROPERTIES AND ENVIRONMENTAL IMPACTS, (2020).
[28] A. International, Standard test method for strength properties of adhesive bonds in shear by compression loadings. Standard D905-08, ASTM International West Conshohocken, Pennsylvania, 2016.
[29] A.S.f. Testing, Materials, Standard practice for estimating the percentage of wood failure in adhesive bonded joints. ASTM D5266-99, ASTM West Conshohocken, Pennsylvania, 2011.
[30] E. Karacebeyli, B. Douglas, CLT handbook-US edition, FPInnovations and Binational Softwood Lumber Council, Point-Claire, Quebec, 2013.
[31] K.S. Sikora, D.O. McPolin, A.M. Harte, Effects of the thickness of cross-laminated timber (CLT) panels made from Irish Sitka spruce on mechanical performance in bending and shear, Constr. Build. Mater. 116 (2016) 141–150.
[32] H.-M. Park, M. Fushitani, H.-S. Byeon, J.-K. Yang, Static bending strength performances of cross-laminated wood panels made with six species, Wood Fiber Sci. 48 (2) (2016) 68–80.
[33] M. Mohamadzadeh, D. Hindman, Mechanical performance of yellow-poplar cross laminated timber, 2015.

[34] ABAQUS, Dassault Systemes, 2017.
[35] R.J. Ross, Wood handbook: wood as an engineering material, USDA Forest Service, Forest Products Laboratory, General Technical Report FPL-GTR-190, 2010: 509 p. 1 v. 190, 2010.
[36] M. Gong, D. Tu, L. Li, Y. Chui, Planar shear properties of hardwood cross layer in hybrid cross laminated timber, ISCHP 2015 (2015) 85–90.
[37] P.P. Camanho, C.G. Dávila, Mixed-mode decohesion finite elements for the simulation of delamination in composite materials, 2002.
[38] E. Barbero, F. Cosso, R. Roman, T. Weadon, Determination of material parameters for Abaqus progressive damage analysis of E-glass epoxy laminates, Compos. B Eng. 46 (2013) 211–220.
[39] E. Guntekin, S. Ozkan, T. Yilmaz, Prediction of bending properties for beech lumber using stress wave method, Maderas, Ciencia y tecnología 16 (1) (2014) 93–98.
[40] K. Frühwald, G. Schickhofer, Strength grading of hardwoods, in: Proceedings of the 14th International Symposium on Nondestructive Testing of Wood, 2005, pp. 199–210.
[41] R.E. Hernández, Influence of accessory substances, wood density and interlocked grain on the compressive properties of hardwoods, Wood Sci. Technol. 41 (3) (2007) 249.
[42] E.A. Okkonen, B.H. River, Factors affecting the strength of block-shear specimens, Review Process: Non-Refereed (Other), 1988.